Fast High-Quality Three-Dimensional Reconstruction from Compressive Observation of Phased Array Weather Radar

Ryosuke Kawami*, Hidetomo Kataoka*, Daichi Kitahara*, Akira Hirabayashi*,
Takashi Ijiri†, Shigeharu Shimamura‡, Hiroshi Kikuchi§, and Tomoo Ushio§
*Graduate School of Information Science and Engineering, Ritsumeikan University, Kusatsu, Shiga, Japan
†Department of Information Science and Engineering, Shibaura Institute of Technology, Koto, Tokyo, Japan
‡Graduate School of Engineering, Osaka University, Suita, Osaka, Japan
§Department of Aerospace Engineering, Tokyo Metropolitan University, Hino, Tokyo, Japan

***Abstract*—Phased array weather radar (PAWR) is capable of spatially and temporally high resolution observation. This means that a PAWR generates a huge amount of observation data, say 500 megabytes in every 30 seconds. To transfer this big data in a public internet line, this paper proposes a fast 3D compressive sensing method for PAWR. The proposed method reconstructs the original data, from compressed data, as the minimizer of a convex function which evaluates the local similarity in the spatial domain and the sparsity in the frequency domain. By combining blockwise optimization with Nesterov's acceleration, we obtain an approximate solution of the above convex optimization problem at high speed. Numerical simulations show that the proposed method outperforms conventional reconstruction methods.**

I. Introduction

One of the extreme weather events is torrential rainfall caused by quick growth of cumulonimbus clouds. Recently, the occurrence frequency of torrential rainfall is increasing [1], but the spatial and temporal resolution of classical parabolic radars is not sufficient to observe such extreme weather events. Phased array weather radar (PAWR) was developed [2], [3] for accurate weather observation. The PAWR system developed in Osaka University can scan atmosphere within a hemisphere of a radius 60 kilometers in 30 seconds, and numbers of sampling points in range, azimuth, and elevation directions are 600, 300, and 110, respectively [3]. The measurements include thirteen aspects of weather phenomena, and the total data size for each single revolution of the PAWR is 490.9 megabytes. Therefore, if all measurements were transferred without any compression technique, the required transfer rate is 131 megabits per second. To this end, the current PAWR system exploits a private internet line with some cost.

In order to use a public internet line for real time transfer, the PAWR data has to be efficiently compressed. For example, when we use a public internet line whose transfer rate is 35 megabits per second, not only the data size must be reduced to less than about $1/4$, but also the original PAWR data has to be reconstructed from the compressed data at high speed. For solving such issues, we can use compressive sensing [4]–[6] which was first applied to radars for hard targets [7]–[9] and then applied to weather radars [10]–[15]. For reconstruction of three-dimensional (3D) tensor data from compressed one, Mishra *et al*. used a low-rank matrix approximation technique [12]. Shimamura *et al*. proposed a one-dimensional (1D) reconstruction algorithm which promotes the sparsity of 1D vector data in the frequency domain [13] where a discrete cosine transform (DCT) or a discrete wavelet transform (DWT) is used as a mapping into the frequency domain. In [14], the present authors proposed a two-dimensional (2D) reconstruction algorithm which promotes the local similarity and the sparsity of 2D matrix data in the spatial and frequency domains, respectively. Recently, we proposed a 3D reconstruction algorithm [15] where the compressed data is created from only the measurements in the troposphere. This algorithm outperformed 2D algorithms [12], [14], but the computational time is too long for real time transfer of the data.

In this paper, to reduce the computational time of the 3D reconstruction in [15], we propose a fast blockwise algorithm. We divide compressed data into some small blocks and then reconstruct original data by minimizing the cost in [15] for every block with the use of the simultaneous direction method of multipliers (SDMM) [16].[1] Since the size of the optimization problem in each block is very small as compared to that of the original problem, the total reconstruction time is dramatically shortened with less quality degradation. Moreover, we improve the convergence rate of SDMM by Nesterov's acceleration technique [18]–[21]. In [20], it is proven that the convergence rate of ADMM can be improved by using Nesterov's acceleration if a cost function is strongly convex. Although the cost in [15] is not strongly convex, we apply this technique to our algorithm. Numerical simulations show that the proposed method, combined with blockwise optimization and Nesterov's acceleration, outperforms the conventional 2D reconstruction algorithms [12], [14] with less computational time.

The rest of this paper is organized as follows. Section II summarizes our 3D compressive sensing scheme for PAWR [15]. Section III presents the proposed fast blockwise reconstruction algorithm. Section IV shows the effectiveness of the proposed reconstruction algorithm in numerical simulations. Finally, Section V concludes this paper.

[1] It is a kind of the alternative direction method of multipliers (ADMM) [17].

II. 3D Compressive Sensing for PAWR Data

In this section, we summarize our 3D compressive sensing scheme recently proposed in [15]. In the following, we focus on the reflection intensity among thirteen parameters observed by the PAWR because the other parameters can be handled in a similar way. The reflection intensities are observed as a 3D tensor $\boldsymbol{X}_0 \in \mathbb{R}^{N_H \times N_V \times N_W}$, and we denote by $x_0[n_H, n_V, n_W]$ the (n_H, n_V, n_W) entry of $\boldsymbol{X}_0$, where $1 \leq n_H \leq N_H := 600$, $1 \leq n_V \leq N_V := 300$, and $1 \leq n_W \leq N_W := 110$ (i.e., the number of measurements is $N := N_H N_V N_W = 19{,}800{,}000$).

A. Data Compression by Random Sampling in Troposphere

The PAWR observes the reflection intensities within a hemisphere of a radius 60 kilometers. This hemisphere includes the out of the troposphere and $x_0[n_H, n_V, n_W]$ should be 0 there. We use this knowledge for both sampling and reconstruction. Let H_{tro} be the height of the troposphere, where the curvature of the earth is not taken into account. In order to compress the original data $\boldsymbol{X}_0$, we randomly select $M\,(< N)$ measurements within areas whose height is lower than H_{tro} and then convert $(N-M)$ non-selected measurements into 0. This compression process is denoted by $\mathcal{A} : \mathbb{R}^{N_H \times N_V \times N_W} \to \mathbb{R}^{N_H \times N_V \times N_W}$, the compressed data is expressed as $\boldsymbol{Y} := \mathcal{A}(\boldsymbol{X}_0)$, and the compression ratio is defined by $\alpha := M/N \in (0, 1)$.

An example of a pair of the original observed data $\boldsymbol{X}_0$ and the compressed data $\boldsymbol{Y}$ is shown in Fig. 1, where slices of the 10th elevation angle are extracted from the entire 3D tensors. The original data $\boldsymbol{X}_0$ was acquired on May 10th, 2013 by the PAWR equipped at Osaka University in Suita Campus, Japan, and the compressed data $\boldsymbol{Y}$ retains only 25% measurements among $\boldsymbol{X}_0$. We recover the missing measurements from the remaining ones via convex optimization in the next section.

B. 3D Reconstruction from Compressed Data

To reconstruct the complete measurements $\boldsymbol{X}_0$ from the randomly selected ones $\boldsymbol{Y}$, we exploit four characteristics of $\boldsymbol{X}_0$. First, measurements outside of the troposphere are 0 as mentioned before. Let us denote the set of all $\boldsymbol{X} \in \mathbb{R}^{N_H \times N_V \times N_W}$ satisfying this condition by S. Second, observation of $\boldsymbol{X}$ should be consistent with $\boldsymbol{Y}$. Third, the reflection intensities are locally similar because rain falling areas exist continuously. Fourth, we suppose that $\boldsymbol{X}_0$ can be sparsely described by some appropriate transformation, e.g., DCT.

On the basis of the above characterizations, we define

$$J(\boldsymbol{X}) := \frac{1}{2}\|\mathcal{A}(\boldsymbol{X}) - \boldsymbol{Y}\|_2^2 + \lambda_1 TV_1(\boldsymbol{X}) + \lambda_2 \|\mathcal{C}(\boldsymbol{X})\|_1,$$

where $\|\boldsymbol{X}\|_2^2 := \sum_{n_H=1}^{N_H}\sum_{n_V=1}^{N_V}\sum_{n_W=1}^{N_W} |x[n_H, n_V, n_W]|^2$, $\|\boldsymbol{X}\|_1 := \sum_{n_H=1}^{N_H}\sum_{n_V=1}^{N_V}\sum_{n_W=1}^{N_W} |x[n_H, n_V, n_W]|$,

$$\begin{aligned} TV_1(\boldsymbol{X}) := &\sum_{n_H=1}^{N_H-1}\sum_{n_V=1}^{N_V}\sum_{n_W=1}^{N_W} |x[n_H+1, n_V, n_W] - x[n_H, n_V, n_W]| \\ &+ \sum_{n_H=1}^{N_H}\sum_{n_V=1}^{N_V-1}\sum_{n_W=1}^{N_W} |x[n_H, n_V+1, n_W] - x[n_H, n_V, n_W]| \\ &+ \sum_{n_H=1}^{N_H}\sum_{n_V=1}^{N_V}\sum_{n_W=1}^{N_W-1} |x[n_H, n_V, n_W+1] - x[n_H, n_V, n_W]|, \end{aligned}$$

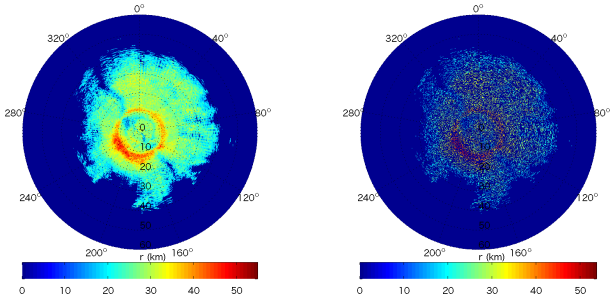

(a) Original observed data (b) Compressed data

Fig. 1. Original and compressed data.

$\mathcal{C} : \mathbb{R}^{N_H \times N_V \times N_W} \to \mathbb{R}^{N_H \times N_V \times N_W}$ is the 3D DCT, $\lambda_1 > 0$, and $\lambda_2 > 0$. We recover the entire reflection intensity $\boldsymbol{X}_0$ by

$$\boldsymbol{X}^* := \operatorname*{argmin}_{\boldsymbol{X} \in S} J(\boldsymbol{X}). \tag{1}$$

In (1), J is a convex function and S is a convex set. Hence, this minimization problem is a convex optimization problem and can be solved by the simultaneous direction method of multipliers (SDMM), which is a special version of the alternative direction method of multipliers (ADMM), as follows.

Let $\boldsymbol{x} := \mathrm{vec}(\boldsymbol{X}) \in \mathbb{R}^N$ be a vectorized version of a 3D tensor $\boldsymbol{X} \in \mathbb{R}^{N_H \times N_V \times N_W}$, and the inverse mapping of vec is denoted by ten (i.e., $\boldsymbol{X} = \mathrm{ten}(\boldsymbol{x})$). Let $A \in \mathbb{R}^{N \times N}$ be a diagonal matrix which converts the values of non-selected components of $\boldsymbol{x}$ into 0 while retaining the other values. Define

$$D_{N_H} := \begin{pmatrix} -1 & 1 & 0 & \dots & 0 \\ 0 & -1 & 1 & \dots & 0 \\ \vdots & \ddots & \ddots & \ddots & \vdots \\ 0 & \dots & 0 & -1 & 1 \end{pmatrix} \in \mathbb{R}^{(N_H-1)\times N_H},$$

and define $D_{N_V} \in \mathbb{R}^{(N_V-1)\times N_V}$ and $D_{N_W} \in \mathbb{R}^{(N_W-1)\times N_W}$ in the same way. The identity matrix and the 1D DCT matrix of size $K \times K$ are denoted by I_K and C_K, respectively. By defining matrices, with the use of the Kronecker product $\otimes$, as

$$\begin{cases} L_1 := I_{N_W} \otimes I_{N_V} \otimes I_{N_H}, & L_2 := I_{N_W} \otimes I_{N_V} \otimes D_{N_H}, \\ L_3 := I_{N_W} \otimes D_{N_V} \otimes I_{N_H}, & L_4 := D_{N_W} \otimes I_{N_V} \otimes I_{N_H}, \\ L_5 := C_{N_W} \otimes C_{N_V} \otimes C_{N_H}, & L_6 := I_{N_W} \otimes I_{N_V} \otimes I_{N_H}, \end{cases}$$

and defining $g_1(\boldsymbol{y}_1) := \frac{1}{2}\|A\boldsymbol{y}_1 - \mathrm{vec}(\boldsymbol{Y})\|_2^2$, $g_i(\boldsymbol{y}_i) := \lambda_1\|\boldsymbol{y}_i\|_1$ $(i = 2, 3, 4)$, $g_5(\boldsymbol{y}_5) := \lambda_2\|\boldsymbol{y}_5\|_1$, $g_6(\boldsymbol{y}_6) := 0$ if $\mathrm{ten}(\boldsymbol{y}_6) \in S$, and $g_6(\boldsymbol{y}_6) := \infty$ if $\mathrm{ten}(\boldsymbol{y}_6) \notin S$, a vectorized version of $\boldsymbol{X}^*$ in (1) is expressed as

$$\boldsymbol{x}^* = \operatorname*{argmin}_{\boldsymbol{x} \in \mathbb{R}^N} \sum_{i=1}^{6} g_i(L_i \boldsymbol{x}). \tag{2}$$

The vector $\boldsymbol{x}^*$ in (2) can be computed by SDMM as shown in Algorithm 1, and the entire reflection intensity is reconstructed as $\boldsymbol{X}^* = \mathrm{ten}(\boldsymbol{x}^*)$. In Algorithm 1, $Q := \sum_{i=1}^{6} L_i^\top L_i \in \mathbb{R}^{N \times N}$ is invertible and the closed form of Q^{-1} can be derived in a similar way as in [14] without any product of huge matrices of size $N \times N$. Moreover, every proximity operator $\mathrm{prox}_{\gamma g_i}$ $(i = 1, 2, \dots, 6)$ can be easily derived (see, e.g., [22]).

Algorithm 1: 3D Reconstruction Method for PAWR Data

Input: $\boldsymbol{Y} \in \mathbb{R}^{N_H \times N_V \times N_W}$ and $\gamma \in (0, \infty)$

$\boldsymbol{y}_{i,0} \leftarrow L_i \mathrm{vec}(\boldsymbol{Y})$ and $\boldsymbol{z}_{i,0} \leftarrow \boldsymbol{0} \quad (i = 1, 2, \ldots, 6)$

$k \leftarrow 1$

while a stopping condition is not met **do**

$\boldsymbol{x}_k \leftarrow Q^{-1} \sum_{i=1}^{6} L_i^\top (\boldsymbol{y}_{i,k-1} - \boldsymbol{z}_{i,k-1})$

$\boldsymbol{y}_{i,k} \leftarrow \mathrm{prox}_{\gamma g_i}(L_i \boldsymbol{x}_k + \boldsymbol{z}_{i,k-1}) \quad (i = 1, 2, \ldots, 6)$

$\boldsymbol{z}_{i,k} \leftarrow \boldsymbol{z}_{i,k-1} + L_i \boldsymbol{x}_k - \boldsymbol{y}_{i,k} \quad (i = 1, 2, \ldots, 6)$

$k \leftarrow k + 1$

end while

III. Acceleration of 3D Reconstruction by Blockwise Optimization and Nesterov's Technique

In this section, we accelerate the 3D reconstruction algorithm (Algorithm 1) in consideration of the data acquisition process of the PAWR. In the PAWR, a matrix $X_0[:, n_V, :] \in \mathbb{R}^{N_H \times N_W}$ is acquired at the same time, and hence by acquiring $X_0[:, n_V, :]$ $(n_V = 1, 2, \ldots, N_V)$ in sequence and combining them, a 3D tensor $\boldsymbol{X}_0 \in \mathbb{R}^{N_H \times N_V \times N_W}$ is generated.

In order to accelerate Algorithm 1 in consideration of the above data acquisition process, we divide the original data $\boldsymbol{X}_0$ and the compressed data $\boldsymbol{Y}$ into N_V/s blocks $\boldsymbol{X}_{0,l} := (X_0[:, (l-1)s+1, :], X_0[:, (l-1)s+2, :], \ldots, X_0[:, ls, :]) \in \mathbb{R}^{N_H \times s \times N_W}$ and $\boldsymbol{Y}_l := \mathcal{A}_l(\boldsymbol{X}_{0,l})$ $(l = 1, 2, \ldots, N_V/s)$. The compression processes $\mathcal{A}_l : \mathbb{R}^{N_H \times s \times N_W} \to \mathbb{R}^{N_H \times s \times N_W}$ have the same compression ratio, i.e., we randomly select sM/N_V measurements from each block $\boldsymbol{X}_{0,l}$ within areas whose height is lower than H_{tro}. Then we approximate the desired tensor $\boldsymbol{X}^*$ in (1) with $(\boldsymbol{X}_1^*, \boldsymbol{X}_2^*, \ldots, \boldsymbol{X}_{N_V/s}^*) \in \mathbb{R}^{N_H \times N_V \times N_W}$ by solving blockwise optimization problems:

$$\boldsymbol{X}_l^* := \operatorname*{argmin}_{\boldsymbol{X}_l \in \widehat{S}} J_l(\boldsymbol{X}_l) \qquad (l = 1, 2, \ldots, N_v/s), \tag{3}$$

where

$$J_l(\boldsymbol{X}_l) := \frac{1}{2} \|\mathcal{A}_l(\boldsymbol{X}_l) - \boldsymbol{Y}_l\|_2^2 + \lambda_1 TV_1(\boldsymbol{X}_l) + \lambda_2 \|\mathcal{C}(\boldsymbol{X}_l)\|_1$$

and $\widehat{S}$ denotes the set of $\boldsymbol{X}_l \in \mathbb{R}^{N_H \times s \times N_W}$ whose all measurements outside of the troposphere are 0. Each small optimization problem in (3) is solved by SDMM in the same way as in Algorithm 1, and $\boldsymbol{X}_l^*$ is reconstructed as $\boldsymbol{X}_l^* = \mathrm{ten}(\boldsymbol{x}_l^*)$.

Moreover, we improve the convergence rate of Algorithm 1 by Nesterov's acceleration technique [18]–[21]. In [20], Goldstein *et al*. proposed Fast ADMM as an accelerated variant of ADMM, and the convergence rate is improved from $\mathcal{O}(1/k)$ to $\mathcal{O}(1/k^2)$ for a strongly convex optimization problem, where the convergence is defined for the cost of the dual problem. Fortunately SDMM is just a special version of ADMM, and hence we apply Nesterov's acceleration technique to dual variables in accordance with [20] (see Algorithm 2). Although the cost function J_l is not strongly convex, we can confirm the notable improvement of the reconstruction time in numerical simulations (see Section IV). Note that since Algorithm 2 can be implemented for several blocks in parallel, graphics processing unit (GPU) is suitable for incorporation of the proposed 3D reconstruction into the PAWR system.

Algorithm 2: Fast Blockwise 3D Reconstruction Method

Input: $\boldsymbol{Y}_l \in \mathbb{R}^{N_H \times s \times N_W}$ and $\gamma \in (0, \infty)$

$\boldsymbol{y}_{i,0} \leftarrow L_i \mathrm{vec}(\boldsymbol{Y}_l)$ and $\boldsymbol{z}_{i,0} \leftarrow \boldsymbol{0} \quad (i = 1, 2, \ldots, 6)$

$\boldsymbol{y}_{i,\frac{1}{2}} \leftarrow \boldsymbol{y}_{i,0}$ and $\boldsymbol{z}_{i,\frac{1}{2}} \leftarrow \boldsymbol{z}_{i,0} \quad (i = 1, 2, \ldots, 6)$

$\alpha_0 \leftarrow 1$ and $k \leftarrow 1$

while a stopping condition is not met **do**

$\boldsymbol{x}_k \leftarrow Q^{-1} \sum_{i=1}^{6} L_i^\top (\boldsymbol{y}_{i,k-\frac{1}{2}} - \boldsymbol{z}_{i,k-\frac{1}{2}})$

$\boldsymbol{y}_{i,k} \leftarrow \mathrm{prox}_{\gamma g_i}(L_i \boldsymbol{x}_k + \boldsymbol{z}_{i,k-\frac{1}{2}}) \quad (i = 1, 2, \ldots, 6)$

$\boldsymbol{z}_{i,k} \leftarrow \boldsymbol{z}_{i,k-\frac{1}{2}} + L_i \boldsymbol{x}_k - \boldsymbol{y}_{i,k} \quad (i = 1, 2, \ldots, 6)$

$\alpha_k \leftarrow \frac{1+\sqrt{1+4\alpha_{k-1}^2}}{2}$

$\boldsymbol{y}_{i,k+\frac{1}{2}} \leftarrow \boldsymbol{y}_{i,k} + \frac{\alpha_{k-1}-1}{\alpha_k}(\boldsymbol{y}_{i,k} - \boldsymbol{y}_{i,k-1}) \quad (i = 1, 2, \ldots, 6)$

$\boldsymbol{z}_{i,k+\frac{1}{2}} \leftarrow \boldsymbol{z}_{i,k} + \frac{\alpha_{k-1}-1}{\alpha_k}(\boldsymbol{z}_{i,k} - \boldsymbol{z}_{i,k-1}) \quad (i = 1, 2, \ldots, 6)$

$k \leftarrow k + 1$

end while

IV. Simulations

To show the effectiveness of the proposed method, we conducted simulations using the data shown in Figs. 2 and 3. The simulations were conducted using Matlab on iMac (OS 10.10, Intel Core i5, 2.7GHz, 8GB). The compressed data $\boldsymbol{Y}$ is generated with compression ratio $\alpha = 0.25$, where the parameter H_{tro} was set as 15 kilometers. Each block $\boldsymbol{Y}_l$ is constructed by $s = 4$ slices.[2] Algorithm 2 reconstructed the entire 3D data from $\boldsymbol{Y}$ with the use of $\gamma = 2, \lambda_1 = 0.05$ and $\lambda_2 = 0.2$. The normalized errors, computed by $\|\boldsymbol{X}^* - \boldsymbol{X}_0\|_2 / \|\boldsymbol{X}_0\|_2$, were 10.14% for Data 1 and 10.15% for Data 2. Figs. 2(d) and 3(d) show slices of the 10th elevation angle extracted from the reconstructed data $\boldsymbol{X}^*$. Figs. 2(g) and 3(g) show their magnifications. The normalized errors of these slices were 10.14% for Data 1 and 9.07% for Data 2, as described in the captions too.

For comparison, we also reconstructed the entire measurements by the authors' method in [14] and Mishra's method in [12], which are called Conventional 1 and Conventional 2, respectively. Since these methods are for 2D sampling and reconstruction, simulations were done slice-by-slice for each elevation angle. Even though measurements are not the same as those for the proposed method, the compression rate was fixed by $\alpha = 0.25$. The normalized errors of the reconstructed entire 3D data by Conventional 1 were 13.34% for Data 1 and 13.61% for Data 2. Those by Conventional 2 were 16.65% for Data 1 and 16.43% for Data 2. The reconstruction results of the 10th elevation angle and their magnifications are shown in Figs. 2(e), (f), (h), (i) and 3(e), (f), (h), (i). For Data 1, the normalized errors of these slices were 13.64% by Conventional 1 and 17.58% by Conventional 2. For Data 2, the normalized errors of these slices were 11.88% by Conventional 1 and 16.36% by Conventional 2. These results show that the proposed method outperforms the conventional methods.

Next, we measured the computational times of the while loops in Algorithms 1 and 2 in cases that Nesterov's technique

[2] $s = 4$ achieved the highest reconstruction accuracy among $\{2, 3, 4, 5, 6\}$.

TABLE I
COMPUTATIONAL TIME OF THE PROPOSED METHOD FOR DATA 1

	No block 3D and Nesterov	Only block 3D	Only Nesterov	Block 3D and Nesterov
Computational time (sec)	43,111	7,241	3,828	1,392 (782)
Error (%)	9.81	9.92	9.99	10.14

is used and not used. Table I shows each computational time for Data 1, where the value in the bracket is the computational time implemented by Python (Cython). We can observe that the method applying both the block 3D reconstruction and Nesterov's technique is the fastest. This method is approximately 30.8 times faster than the method applying neither accelerating technique. In addition, the method implemented by Python is further 1.8 times faster. Table I also shows the reconstruction accuracy of each method. Although the reconstruction accuracy slightly goes down by applying the accelerating techniques, this deterioration is within permissible range. Thus, the block 3D reconstruction and Nesterov's technique are very effective for accelerating our method. The computational times of Conventional 1 and Conventional 2 were 13,581 and 6,707 seconds, respectively. Therefore, the proposed method reconstructs the data with approximately 5.0 times less computational time than 2D methods.

Yet, to complete the reconstruction for thirteen parameters of the PAWR, the proposed method requires approximately 10,000 seconds. Since the reconstruction should be completed within 30 seconds, 333 times acceleration is required approximately. Note that since reconstruction for each block can be performed in a parallel way, such a computation using graphics processing unit (GPU) is very effective for further acceleration of the proposed method. In this simulation, the number of slice s is set as 4, which means that 3D data is divided into 75 blocks. Hence, the reconstruction time of one block is approximately 10.4 seconds. If the each block is reconstructed by separate calculators in a parallel way, the one parameter of PAWR data can be reconstructed in real time. In this case, to complete the reconstruction for all parameters of the PAWR in real time, approximately 4.5 times acceleration is required.

V. CONCLUSION

This paper has proposed a fast reconstruction algorithm in 3D compressive sensing for the PAWR. First, we summarized our 3D compressive sensing scheme combined with random sampling in the troposphere and convex optimization. Then, for shortening the reconstruction time, we proposed blockwise optimization, where the measurements are divided into some blocks, and each block is reconstructed separately. Since reconstruction for each block can be performed in a parallel way, our method can be further accelerated. Moreover, we applied Nesterov's technique to SDMM and the convergence rate is improved in numerical simulations. By applying these acceleration techniques, the proposed method reconstructed the original 3D data with approximately 5.0 and 30.8 times less computational time than 2D and 3D methods, respectively.

ACKONWEDGMENT

The authors are grateful to Prof. Jeremy White in Ritsumeikan University for improving English expressions.

REFERENCES

[1] Committee on Extreme Weather Events and Climate Change Attribution, *Attribution of Extreme Weather Events in the Context of Climate Change.* Washington D.C., WA: The National Academy Press, 2016.

[2] F. Mizutani, M. Wada, H. Marui, H. Handa, T. Ushio, S. Satoh, and Toshio Iguchi, "Development of active phased array weather radar," in *Proceedings of 35th Conference on Radar Meteorology*, 2011.

[3] E. Yoshikawa, T. Ushio, Z. Kawasaki, S. Yoshida, T. Morimoto, F. Mizutani, and M. Wada, "MMSE beam forming on fast-scanning phased array weather radar," *IEEE Transactions on Geoscience and Remote Sensing*, vol. 51, no. 5, pp. 3077–3088, 2013.

[4] D. Donoho, "Compressed sensing," *IEEE Transactions on Information Theory*, vol. 52, no. 4, pp. 1289–1306, 2006.

[5] E. Candes and M. Wakin, "An introduction to compressive sampling," *IEEE Signal Processing Magazine*, vol. 25, no. 2, pp. 21–30, 2008.

[6] Y. Eldar and G. Kutyniok, *Compressed Sensing: Theory and Applications*, Cambridge, MA: Cambridge University Press, 2011.

[7] R. Baraniuk and P. Steeghs, "Compressive radar imaging," in *Proceedings of IEEE Radar Conference*, 2007, pp. 128–133.

[8] M. A. Herman and T. Strohmer, "High-resolution radar via compressed sensing," *IEEE Transactions on Signal Processing*, vol. 57, no. 6, pp. 2275–2284, 2009.

[9] J. H. Ender, "On compressive sensing applied to radar," *Signal Processing*, vol. 90, no, 5, pp. 1402–1414, 2010.

[10] P. Meischner, Ed., *Weather Radar: Principles and Advanced Applications*, London, UK: Springer-Verlag, 2004.

[11] T. Y. Yu, L. Ding, and S. Ozturk, "Application of compressive sensing to refractivity retrieval with a network of radars," in *Proceedings of IEEE Radar Conference*, 2011, pp. 757–761.

[12] K. V. Mishra, A. Kruger, and W. F. Krajewski, "Compressed sensing applied to weather radar," in *Proceedings of IEEE Geoscience and Remote Sensing Symposium*, 2014, pp. 1832–1835.

[13] S. Shimamura, H. Kikuchi, T. Matsuda, G. Kim, T. Ushio, E. Yoshikawa, and Y. Nakamura, "Large-volume data compression using compressed sensing for meteorological radar," in *Proceedings of 37th Conference on Radar Meteorology*, 2015.

[14] R. Kawami, A. Hirabayashi, N. Tanaka, M. Shibata, T. Ijiri, S. Shimaura, H. Kikuchi, G. Kim, and T. Ushio, "2-Dimensional high-quality reconstruction of compressive measurements of phased array weather radar," in *Proceedings of Asia-Pacific Signal and Information Processing Association Annual Summit and Conference (APSIPA ASC)*, 2016,

[15] R. Kawami, T. Ijiri, A. Hirabayashi, S. Shimaura, H. Kikuchi, and T. Ushio, "3-Dimensional Compressive Sensing and High-Quality Recovery for Phased Array Weather Radar," in *Proceedings of the12nd International Conference on Sampling Theory and Applications (SampTA)*, 2017.

[16] L. Condat, "A generic proximal algorithm for convex optimization—application to total variation minimization," *IEEE Signal Processing Letters*, vol. 21, no. 8, pp. 985–989, 2014.

[17] D. Gabay and B. Mercier, "A dual algorithm for the solution of nonlinear variational problems via finite element approximation," *Computers & Mathematics with Applications*, vol. 2, no. 1, pp. 17–40, 1976.

[18] Y. E. Nesterov, "A method for solving the the convex programming problem with convergence rate $O(1/k^2)$," *Doklady Akademii Nauk SSSR*, vol. 269, no. 3, pp. 543–547, 1983.

[19] A. Beck and M. Teboulle, "A fast iterative shrinkage-thresholding algorithm for linear inverse problems," *SIAM Journal on Imaging Sciences*, vol. 2, no. 1, pp. 182–202, 2009.

[20] T. Goldstein, B. O. Donoghue, S. Setzer, and R. Baraniuk, "Fast Alternating Direction Optimization Methods," *SIAM Journal on Imaging Sciences*, vol. 7, no. 3, pp. 1588–1623, 2014.

[21] M. Yamagishi, D. Kitahara, and I. Yamada, "A fast dual Iterative algorithm for convexly constrained spline smoothing," in *Proceedings of the 41st IEEE International Conference on Acoustics, Speech and Signal Processing (ICASSP)*, 2016, pp. 4538–4542.

[22] P. L. Combettes and J. C. Pesquet, "Proximal splitting methods in signal processing," in *Fixed-Point Algorithms for Inverse Problems in Science and Engineering*, H. H. Bauschke, R. S. Burachik, P. L. Combettes, V. Elser, D. R. Luke, and H. Wolkowicz, Eds. New York, NY: Springer, 2011, pp. 185–212.

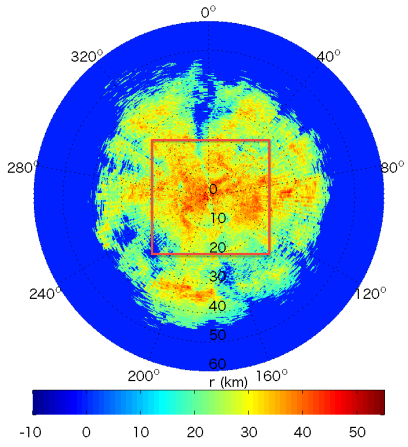

(a) Original observed data

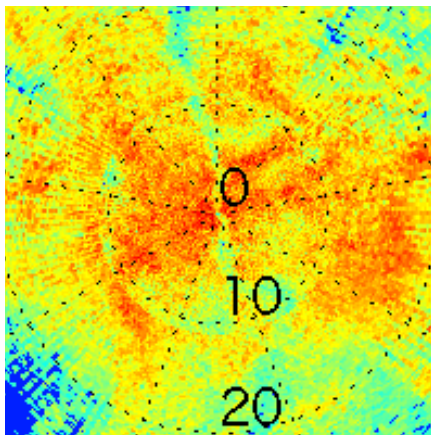

(b) Magnification of red box in (a)

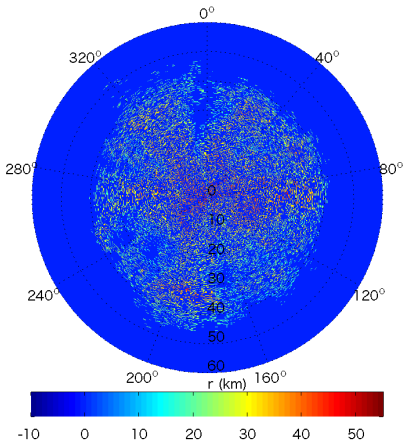

(c) 25% random selected data

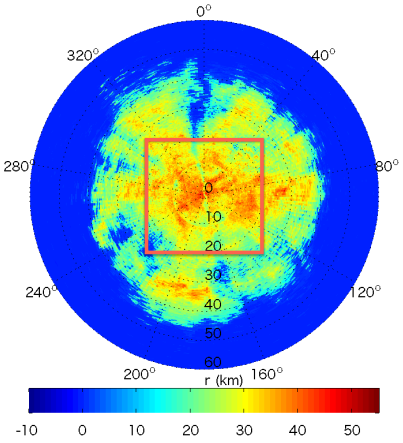

(d) Proposed method (10.14%)

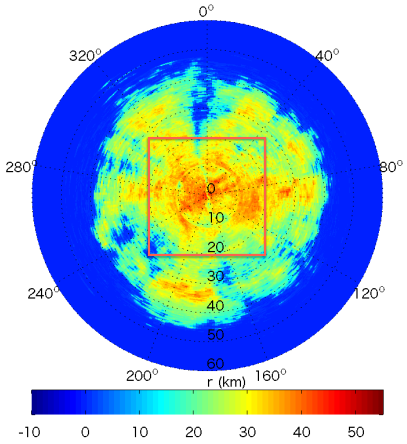

(e) Conventional 1 (13.64%)

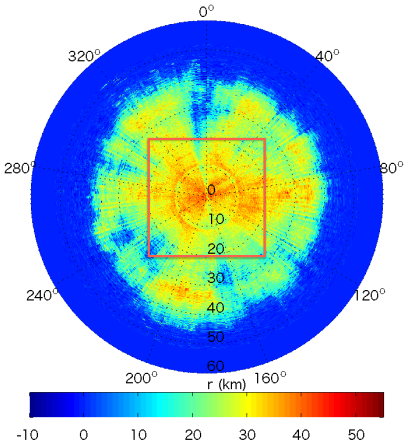

(f) Conventional 2 (17.58%)

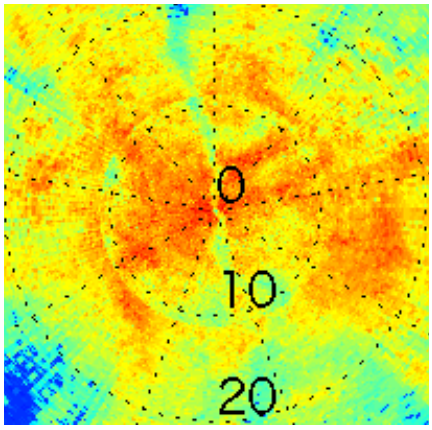

(g) Magnification of red box in (d)

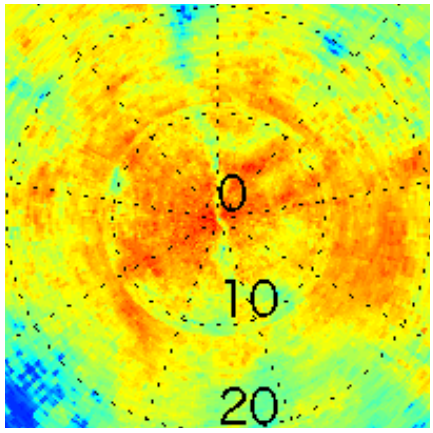

(h) Magnification of red box in (e)

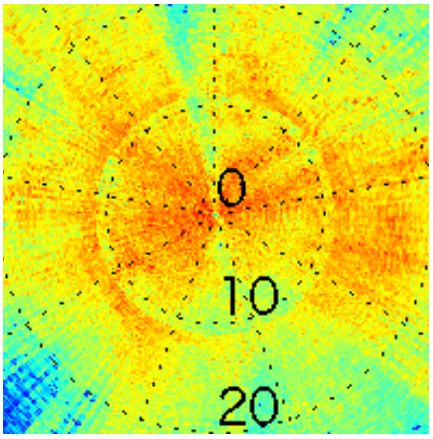

(i) Magnification of red box in (f)

Fig. 2. Simulation results for the reflection intensity observed on June 19th, 2013.

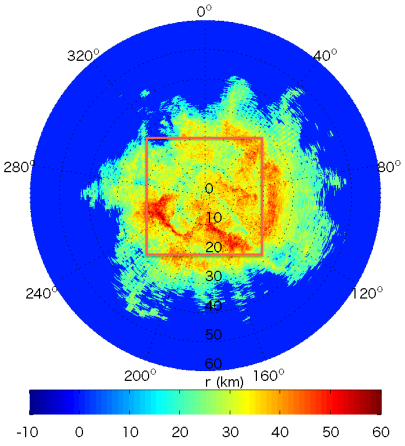

(a) Original observed data

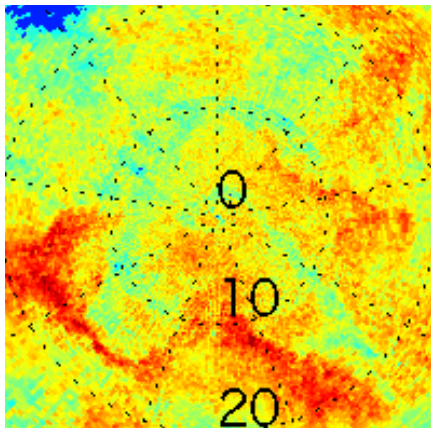

(b) Magnification of red box in (a)

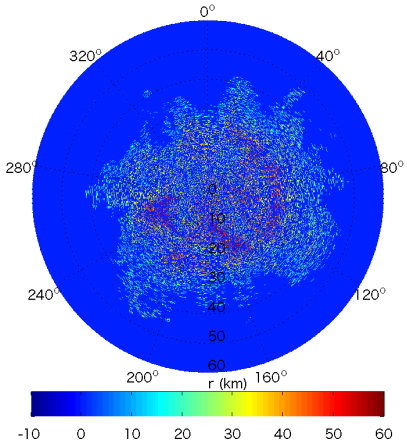

(c) 25% random selected data

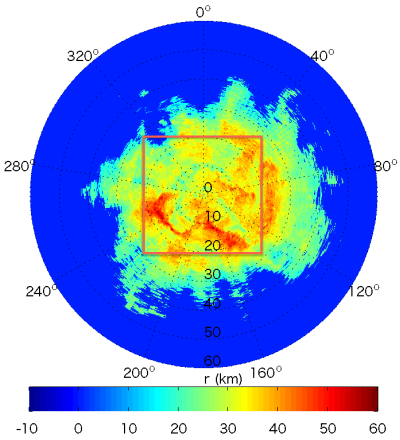

(d) Proposed method (9.07%)

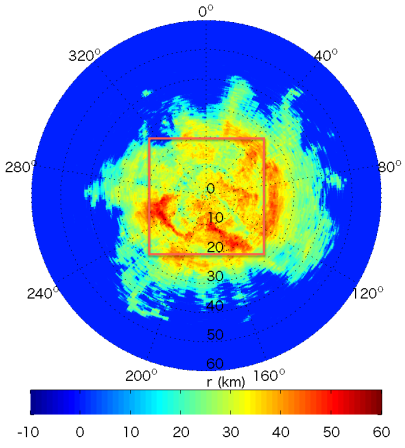

(e) Conventional 1 (11.88%)

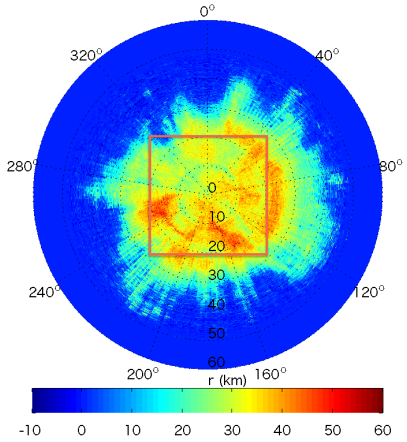

(f) Conventional 2 (16.36%)

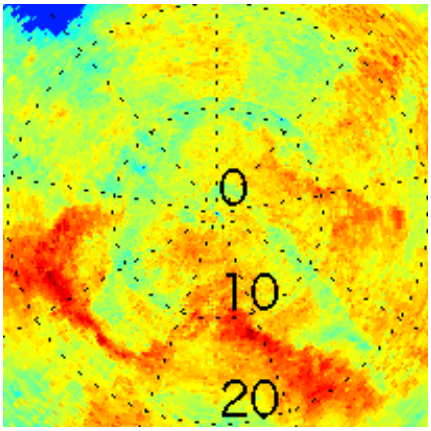

(g) Magnification of red box in (d)

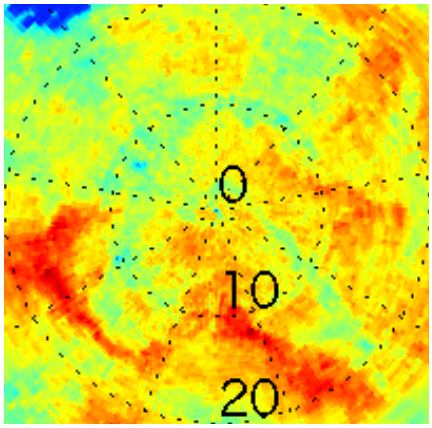

(h) Magnification of red box in (e)

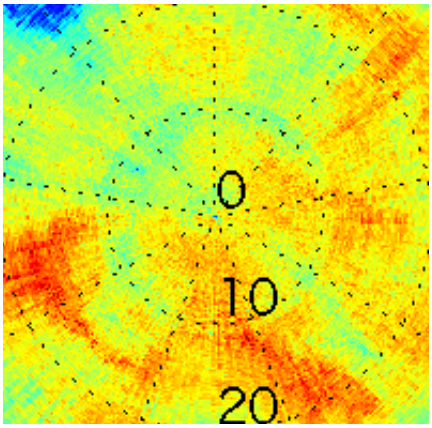

(i) Magnification of red box in (f)

Fig. 3. Simulation results for the reflection intensity observed on March 30th, 2014.